ENVIRONMENTAL RESEARCH
COMMUNICATIONS

INCLUSIVE PUBLISHING
TRUSTED SCIENCE

Part of the
ENVIRONMENTAL RESEARCH
SERIES

PURPOSE-LED
PUBLISHING™

PAPER • **OPEN ACCESS**

Black carbon concentrations and atmospheric forcing in a high-altitude Himalayan valley

To cite this article: Aparna Gupta *et al* 2026 *Environ. Res. Commun.* **8** 035030

Environmental Research Communications

OPEN ACCESS

RECEIVED
16 October 2025

REVISED
27 February 2026

ACCEPTED FOR PUBLICATION
13 March 2026

PUBLISHED
27 March 2026

PAPER

Black carbon concentrations and atmospheric forcing in a high-altitude Himalayan valley

Aparna Gupta[1], **Rakesh Kumar Ranjan**[1,*], **Vrinda Anand**[2], **Abhilash Panicker**[2], **Rajeev Rajak**[1], **Khushboo Sharma**[1,3], **Bidyutjyoti Baruah**[1], **Ankita Roy**[1], **Shruti Dutta**[1] and **Amit Prakash**[4]

[1] Department of Geology, Sikkim University, Gangtok, Sikkim, 737102, India
[2] Indian Institute of Tropical Meteorology, MoES, Govt of India, Pune, 411008, India
[3] International Center for Integrated Mountain Development (ICIMOD), GPO Box 3226, Kathmandu, Nepal
[4] Department of Environmental Science, Tezpur University, Tezpur, Assam, 784028, India
[*] Author to whom any correspondence should be addressed.

E-mail: rkranjan@cus.ac.in

Keywords: Black Carbon, Radiative Forcing, High-altitude aerosols, Eastern Himalaya, BC transport

Supplementary material for this article is available online

Abstract

Black carbon (BC), a strong light-absorbing aerosol, is a significant contributor to atmospheric warming, particularly over high-altitude cryospheric regions. This study presents BC measurements using a seven-wavelength Aethalometer (AE-33), at Yumthang Valley (~3800 m a.s.l.), a high-altitude region in Eastern Himalaya. Monthly mean BC concentrations ranged from 1.04 μg m^{-3} (August) to 9.55 μg m^{-3} (April), with peaks during the pre-monsoon period and minima in the monsoon months. Elevated pre-monsoon concentrations are attributed to regional biomass burning, long-range transport, and seasonally enhanced atmospheric stability, while reduced concentrations during monsoon is due to wet scavenging. Fossil fuel combustion accounts for 58% of the total BC, with peak contribution in February (78%) and lowest in September (40%). Long-range transport models indicate an influx of pollutants from the Indo-Gangetic Plain and adjacent valleys with increased biomass burning activity. Seasonal variations reflect tourism-driven emissions and local biomass burning, with the lowest concentration observed in the early morning hours. The Santa Barbara DISORT Atmospheric Radiative Transfer (SBDART) model results an estimated increase in temperature at rates of 0.83 K day^{-1} in the region due to BC induced atmospheric heating. These results underscore the vulnerability of Himalayan high-altitude valleys to transported pollutants and highlight the importance of BC in altering radiative forcing and accelerating cryospheric melt.

1. Introduction

Black carbon (BC) is a critical atmospheric component produced during the incomplete combustion of biomass, fossil fuels, and biofuels, and it constitutes a major fraction of atmospheric light-absorbing aerosols (Bond *et al* 2013). They have an atmospheric lifetime ranging from a few days to weeks and can be transported over long distances, reaching remote regions such as the Arctic (Stohl *et al* 2006), Antarctic (Tomasi *et al* 2007, Chaubey *et al* 2011) and the Himalaya (Hyvärinen *et al* 2009, Marinoni *et al* 2010, Dumka *et al* 2010). BC is primarily emitted from diesel engines, coal-fired power plants, residential biofuel combustion, open biomass burning, and agricultural residue fires. Biofuel and open-fire emissions together contribute up to ~60% of total BC, although their relative importance varies across urban and remote environments (Ramanathan and Carmichael 2008). BC has been observed in remote mountain and polar regions, for example, in the Andean mountains (Rowe *et al* 2019, Lapere *et al* 2023), European Pyrenees/Alps (Tinorua *et al* 2024), across the Rocky Mountains (Rahimi *et al* 2020), Hindu-Kush Himalaya (Singh *et al* 2023) and on the Tibetan Plateau (Zhao *et al* 2017) demonstrating its long-range transport and cryospheric impacts. The Hindu-Kush Himalaya and Tibetan Plateau (HTP) region with its snow/ice cover is vulnerable because of its positioning between East Asia

and South Asia, two major BC sources (Bond *et al* 2007, Ohara *et al* 2007, Xu *et al* 2009, Lamarque *et al* 2010, Menon *et al* 2010).

BC has a significant influence on the regional and global climate by altering the Earth's radiative balance and atmospheric energy budget (Lau and Kim 2006, Ramanathan and Carmichael 2008, Flanner *et al* 2009, IPCC 2013). It strongly absorbs electromagnetic radiation across wavelengths from ultraviolet (UV) to near-infrared (NIR) due to its chemical structure, optical properties and relatively long atmospheric lifetime (Drinovec *et al* 2015). Such absorption drives several atmospheric feedback mechanisms, such as alterations in the stability of the atmosphere, large-scale circulation regime, rain duration, rain size distribution and overall hydroclimatic variability (Koch and Del Genio 2010). It is also capable of mixing with different primary and secondary chemical species along with acting as substrate/catalyst for atmospheric processes (Wang *et al* 2016). It alters the regional and global climate by absorbing solar radiation, which reduces surface-reaching sunlight and modifies the albedo of clouds and snow (Ramachandran and Rajesh 2007). The BC effect over snow/ice cover has been found to enhance heating in the range of 0.02 to 0.09 Wm^{-2} globally increasing net shortwave radiation at the snow surface by 1 to 3 Wm^{-2} (IPCC 2013). This results in a warming of approximately 0.05 °C-0.3 °C (Ménégoz *et al* 2014) accelerating snow and glacier melt (Déry and Brown 2007, Ménégoz *et al* 2013).

The radiative impact of BC becomes pronounced at higher altitudes due to reduced air density, amplifying atmospheric warming. The vast cryospheric regions of the high-altitude Himalayas, including numerous glaciers, snowfield and snow-covered regions (Kääb *et al* 2012, Ménégoz *et al* 2014) are vulnerable due to high radiation levels and their proximity to anthropogenic BC sources in the Indian subcontinent. This region is directly affected by the northward transport of BC-loaded air masses from the densely polluted Indo-Gangetic plains (IGP) (Lawrence and Lelieveld 2010). Strong convective uplift over the IGP and adjacent tropical landmasses can lift BC above the boundary layer into the entrainment zone (Babu *et al* 2008), where relatively stable atmospheric conditions prolong its residence time and enhance atmospheric heating (Satheesh *et al* 2008, Babu *et al* 2011b).

BC concentration in the atmosphere is therefore a significant constituent influencing large-scale climatic feedback as well as enhancing atmospheric heating, especially in high altitude (>3000 masl) regions. In-situ BC concentration have been reported from the Western Himalaya including Machaoi, Drass valley (0.28 to 3.7 $\mu g\ m^{-3}$) (Romshoo *et al* 2022), Lahaul and Spiti Valley (0.005 to 0.35 $\mu g\ m^{-3}$) (Arun *et al* 2019) and Hanle, Ladakh (0.007 to 0.3 $\mu g\ m^{-3}$) (Nair *et al* 2013). Similar BC concentrations have been reported from other high-altitude region in central Himalaya such as Mount Everest ranging from 0.09 to 2.7 $\mu g\ m^{-3}$ (Kang *et al* 2022), and Yala Glacier ranging from 0.1 to 4 $\mu g\ m^{-3}$ in Langtang Valley, Nepal (Gul *et al* 2021). However, the Eastern Himalaya remains poorly characterized in terms of BC observations at high altitudes, despite being susceptible to transported and local emissions. To the best of our knowledge, no field-based measurements of BC have been reported from any high-altitude location in the Eastern Himalaya. This is in strong contrast to the Western and Central Himalaya, where the *in situ* BC measurements provide valuable insight into BC characteristics, variability and transport mechanisms.

Sikkim, a part of the Eastern Himalaya, is highly vulnerable to the impacts of BC, including accelerated glacier melting and regional climate changes, due to its proximity to major BC source regions such as the IGP. In recent years, BC concentrations have been explored using remote sensing data, which reported an increase of ~7% in BC column optical depth over Sikkim (Agrawal *et al* 2014). The only field-based BC measurements available is for Gangtok, an urban centre (~1700 masl) (Sharma *et al* 2022, Kumar *et al* 2024). To address this, the present study reports two years of *in situ* BC measurements from a remote high-altitude site (Yumthang Valley, ~3800 m a.s.l.) in North Sikkim, Eastern Himalaya. The study investigates the temporal variations in BC concentrations, potential source contributions, and assessment of their radiative impacts in this climate-sensitive cryospheric region. This study will help in the characterisation of BC and understanding its role in changing the radiative balance, and its implications for glacier melt and atmospheric warming in the region. It will also help bridge the data gap for *in situ* BC measurements allowing for understanding the spatial heterogeneity in BC concentration due to regional differences and meteorological influences.

2. Study area

The study was conducted at Yumthang Valley (27.7993°N, 88.7037°E; ~3800 m a.s.l.), located in North Sikkim, south of the Tibetan Plateau in the Eastern Himalaya (figure 1). The valley lies approximately 150 km north of Gangtok, the state capital, and 23 km north of Lachung village, the nearest inhabited settlement. The area experiences distinct seasonal variability influenced by the Southwest Monsoon and mid-latitude westerlies. About 80% of annual precipitation occurs during the monsoon season, mainly as rainfall, whereas winter precipitation is dominated by snowfall (Kakkar *et al* 2022). Mean temperatures range from 13.9 °C in July to

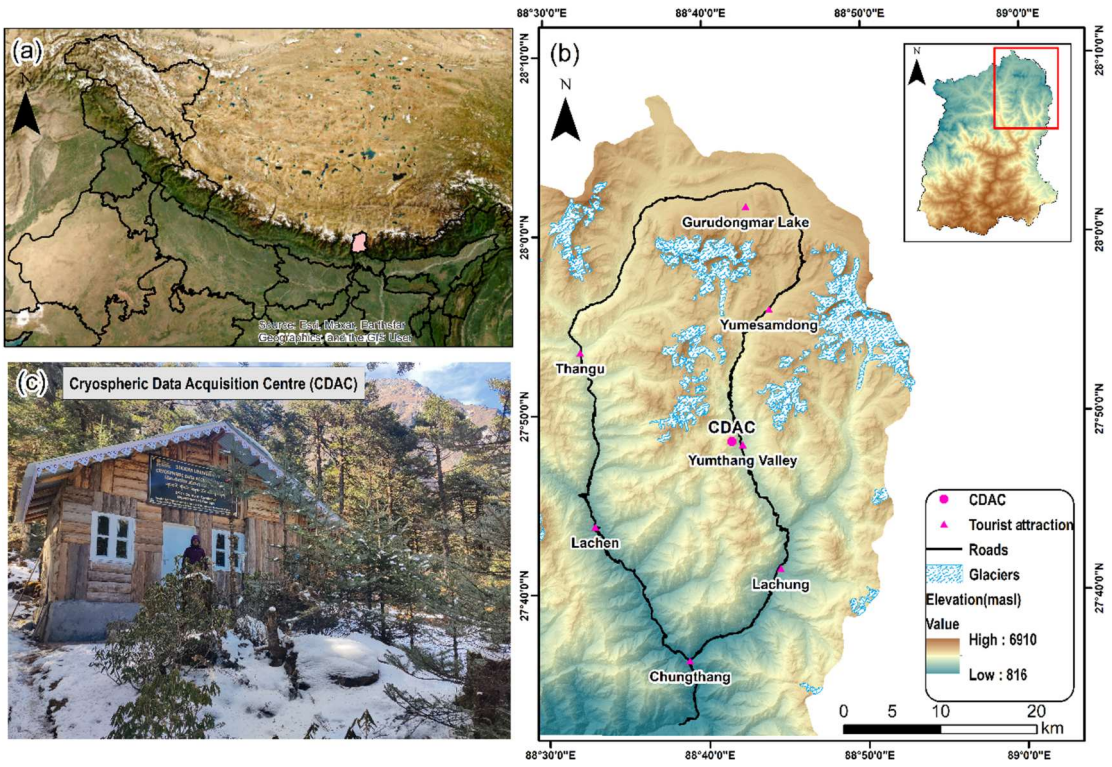

Figure 1. Study area map illustrating the geographical context of the research site. (a) shows the part of political boundary of India with Sikkim highlighted in pink. (b) zooms into Northern Sikkim (marked by a red box) with glacier boundaries, major tourist attractions (pink triangles), road networks (black lines), and the Cryospheric Data Acquisition Centre (CDAC) (pink circle) where aethalometer is installed. (c) provides a close-up view of the high-altitude CDAC research facility. Source: Esri, Maxar, Earthstar Geographics, and the GIS User Community.

−17.1 °C in February, and the annual mean relative humidity is approximately 80.8%, varying from ∼45% in December to >89% during monsoon months .

Topographically, the site lies in the valley floor of a large U-shaped valley bounded by steep mountain ridges. *Lachung Chhu*, originating from glacier-fed meltwaters, flows through the valley, linking the high-altitude basin to downstream inhabited regions. It is a major tourist destination, attracting visitors throughout the year due to its alpine meadows, rhododendron forests, and proximity to snowfields and glaciers. The natural beauty of the region attracts approximately 500,000 visitors during the entire observation period (Market Research and Statistics, Sikkim Tourism). Tourist activity peaks between March and June, but a continuous influx of visitors occurs even during other months, with small temporary roadside stalls operating only during the daytime. Domestic heating using firewood and vehicular traffic in Yumthang and Lachung contribute to localized emissions that, under favourable meteorological and orographic conditions, may be uplifted toward higher elevations. Nonetheless, Yumthang's high-altitude location, situated far from any major industrial or population centers, ensures that observed aerosols predominantly reflect long-range transported pollutants, particularly those originating from the IGP. This makes the site ideal for evaluating the efficiency of regional-scale aerosol transport processes and for characterizing the background atmospheric composition of the Eastern Himalaya. Yumthang lies in proximity to the glaciers and remains snow-covered during winter, with snowmelt beginning in late spring. This provides a natural environment for investigating aerosol-snow interactions and radiative effects. The deposition of BC on nearby snow and ice surfaces can lead to significant surface darkening, albedo reduction, and accelerated melt, making this site particularly suitable for assessing BC-induced cryospheric effects in the region.

3. Data & methodology

3.1. Instrumentation and data processing

A dual-spot, multi-wavelength aethalometer (AE-33, Magee Scientific) placed at Cryospheric Data Acquisition Centre (CDAC) (27.7993 °N, 88.7037 °E) in Yumthang valley was used to measure the BC concentrations at a 1-min temporal resolution and at a flow rate of 5 litres per minute from May 2022 to April 2024. The instrument operates across seven optical wavelengths, ranging from near-infrared (370 nm) to near-ultraviolet

(950 nm). It is designed to enable real-time compensation for filter loading effects by comparing light attenuation between a measurement spot and a reference spot. The instrument determines the real-time concentration of optically absorbing aerosols by measuring the rate of change in light attenuation through aerosol-laden filters and is calculated using equation (1), (for details, see (Drinovec *et al* 2015, Magee Scientific 2018)):

$$\mathrm{ATN} = -100 \times \left(\frac{\mathrm{I}}{\mathrm{I}_0}\right) \tag{1}$$

where I represent the intensity of light passing through the aerosol-laden filter and I_0 represents the intensity of light passing through the reference (clean) filter. This attenuation is then used to determine BC concentration by using the mass absorption cross-section (MAC) value (7.77 $m^2\ g^{-1}$ for 880 nm wavelength). The MAC value converts the measured optical attenuation into a mass concentration of BC, expressed by:

$$BC = \frac{\mathrm{b_{abs}}}{\sigma_{\mathrm{abs}}} \tag{2}$$

where b_{abs} represents the absorption coefficient and σ_{abs} is the mass absorption cross-section. By simultaneously sampling from two spots with different aerosol accumulation rates, the AE-33 mathematically adjusts for nonlinearities, providing compensated values for particle light absorption and BC mass concentration. This is calculated using the equation:

$$BC = \frac{S * \left(\Delta \frac{ATN_1}{100}\right)}{F_1(1 - \zeta) * \sigma_{air} * C * (1 - k * ATN_1) * \Delta t} \tag{3}$$

where S is the spot area, F_1 is the measured flow, ζ is the leakage factor, σ_{air} is the mass absorption cross-section, C (set at 2.14) corrects for multiple light scattering effects of the filter fibres (Weingartner *et al* 2003) and *k* is the compensation parameter.

3.2. Source apportionment

3.2.1. Fossil fuels (FF) and biomass burning (BB) source contribution

The Aethalometer model (equation (6)), developed by Sandradewi *et al* (2008), is used to quantify the contributions to total BC mass concentration from the different sources such as fossil fuel and biomass burning based on differences in their wavelength-dependent optical absorption. BC associated with biomass burning exhibits stronger absorption in the UV range whereas BC from fossil fuel is predominantly absorbed at near-infrared wavelengths (Kirchstetter *et al* 2004). The distinction is characterized using the AAE (α), calculated from absorption coefficients at two different wavelengths ($\boldsymbol{\lambda}_1$, $\boldsymbol{\lambda}_2$) (Resquin *et al* 2018). In this study, AAE_{BC} has been calculated following the approach described in (Helin *et al* 2021). The total absorption at a given wavelength is expressed as the sum of contributions from fossil fuel and biomass burning sources:

$$b_{abs}(\lambda) = b_{abs}(\lambda)_{ff} + b_{abs}(\lambda)_{bb} \tag{6}$$

The wavelength dependency of the absorption coefficient for fossil fuel BC is expressed as:

$$\frac{b_{abs}(470)ff}{b_{abs}(950)_{ff}} = \left(\frac{470}{950}\right)^{-\alpha_{ff}} \tag{7}$$

Similarly, for biomass burning BC:

$$\frac{b_{abs}(470)bb}{b_{abs}(950)_{bb}} = \left(\frac{470}{950}\right)^{-\alpha_{bb}} \tag{8}$$

In this study, we have assumed $\boldsymbol{\alpha_{ff}} \sim 1.0$ for fossil fuel and $\boldsymbol{\alpha_{bb}} \sim 2.0$ for biomass burning emissions (Zotter *et al* 2017, Kant *et al* 2020). BB contribution to total BC can be quantified by solving equations (6)–(8) and BC_{ff} is calculated as follows:

$$BC_{ff} = BC - BC_{bb} \tag{9}$$

3.2.2. Concentration weighted trajectory analysis

The HYSPLIT model, developed by NOAA (National Oceanic and Atmospheric Administration) was used to perform backward trajectory while the concentration-weighted trajectory (CWT) analyses to determine the potential sources of BC were performed using TrajStat software package (Wang *et al* 2009. The backward air mass trajectories, generated using the HYSPLIT, were combined with long-term air pollution data using TrajStat to assign a weighted concentration to each grid by averaging the concentrations of air mass trajectories passing through that grid. In CWT (Hsu *et al* 2003), this is mathematically expressed as:

$$Cij = \frac{1}{\sum_{l=1}^{M} \tau_{ijl}} \sum_{l=1}^{M} C_l \tau_{ijl} \quad (10)$$

where C_{ij} is the weighted average concentration in the ijth cell, M is the number of trajectories, C_l is the BC concentration at arrival of trajectory l, and τ_{ijl} is the residence time of trajectory l in the ijth grid cell. A large C_{ij} value signifies that air masses moving through a specific grid cell are highly correlated with high BC concentrations at the receptor site (Wang *et al* 2019).

To determine the sources of BC, HYSPLIT was utilised to compute the 3-day air mass back trajectories at 500 m above ground level (within the atmospheric boundary layer), based on meteorological data from the GDAS global reanalysis dataset. CWT analysis was performed further to determine the dominant transport pathways and potential source regions contributing to BC loading at the receptor site.

3.3. BC radiative forcing

To estimate BC radiative forcing, we utilized the Santa Barbara DISORT Atmospheric Radiative Transfer (SBDART) model (Ricchiazzi *et al* 1998), which performs radiative transfer calculations in both the shortwave (0.2 to 4.0 μm) and longwave (4.0 to 40.0 μm) spectral regions. The SBDART model, based on the discrete ordinate approach, effectively resolves radiative transfer in a vertically stratified, plane-parallel atmosphere, incorporating multiple scattering processes. Its computational efficiency and reliability make it a widely used tool in radiative forcing studies (Krishna *et al* 2019). Key aerosol optical parameters required for radiative transfer modeling include the asymmetry parameter (g), aerosol optical depth (AOD), and single scattering albedo (SSA). These properties were derived using the Optical Properties of Aerosols and Clouds (OPAC) model (Hess *et al* 1998) under varying relative humidity conditions representative of Yumthang and have been summarized in table 1. Input variables for OPAC included BC mass concentrations and relative humidity, which were measured on-site and boundary layer height (BLH) which was obtained from ERA5. Based on the measured BC concentrations, the continental average aerosol type was selected for the simulations.

Additionally, essential surface and atmospheric parameters were incorporated into SBDART, including MODIS-derived surface reflectance, water vapour profiles and columnar ozone concentrations. Surface albedo values were obtained from the MODIS MCD43A3 (500 m, Version 6) albedo dataset (Campagnolo *et al* 2016), total column ozone was extracted from the OMI/Aura Level 3 OMTO3e product and water vapour profiles were taken from ERA5. Due to the absence of *in situ* vertical atmospheric profiles, the mid-latitude winter standard atmospheric profile provided by SBDART was adopted. The BC direct radiative forcing (DRF) was computed at hourly intervals and aggregated to obtain monthly estimates. The radiative forcing (ΔF) was calculated by determining the difference in radiative fluxes with and without aerosol presence. The equation used in SBDART for calculating radiative forcing is:

$$\Delta F = (F_{withaerosols}\downarrow - F_{withaerosols}\uparrow) - (F_{withoutaerosols}\downarrow - F_{withoutaerosols}\uparrow) \quad (11)$$

where $F^{\downarrow}_{\text{with aerosols}}$, $F^{\downarrow}_{\text{without aerosols}}$, $F^{\uparrow}_{\text{with aerosols}}$, and $F^{\uparrow}_{\text{without aerosols}}$ denote the downward and upward radiative fluxes with and without aerosol, respectively. The atmospheric forcing, representing energy trapped within the atmosphere, was computed as the difference between TOA and SUR forcings.

The atmospheric heating rate, is used to quantifies either cooling or warming of the atmosphere due to atmospheric aerosol absorption (i.e. DRF_{ATM}) was derived from Liou (2002):

$$\frac{\partial T}{\partial t} = \frac{g}{c_p} * \frac{\Delta F}{\Delta P} \quad (12)$$

where $\partial T/\partial t$ represents the heating rate (K/day), g represents the acceleration due to gravity, C_p represents the specific heat capacity of air at constant pressure (1006 J kg^{-1}·K), and ΔP represents the pressure difference. Estimating BC radiative forcing using OPAC and SBDART involves several uncertainties. These mainly arise from assumptions related to the atmospheric profile, the chosen aerosol type in OPAC, and inaccuracies in measured BC mass concentrations, molecular scattering and absorption. Additional uncertainty arises from surface albedo inputs, as MODIS albedo carries an estimated ~6% error that affects both Top-of-Atmosphere (TOA) and surface forcing (SUR) calculations (Strahler *et al* 1999). Choices made in selecting the atmospheric profile and aerosol type also impact the results. When combined, these factors can contribute to an overall uncertainty of ~15% in the radiative forcing estimates (Srivastava *et al* 2011), with an overall accuracy of about ±2 W m^{-2} (Satheesh and Srinivasan 2006).

4. Results and discussion

4.1. Temporal dynamics of BC

The annual mean BC concentration in Yumthang Valley during May 2022-April 2024 was found to be 5.07 μg m^{-3} (SD = 16.54 μg m^{-3}). The reported BC concentrations are comparable with measurements at

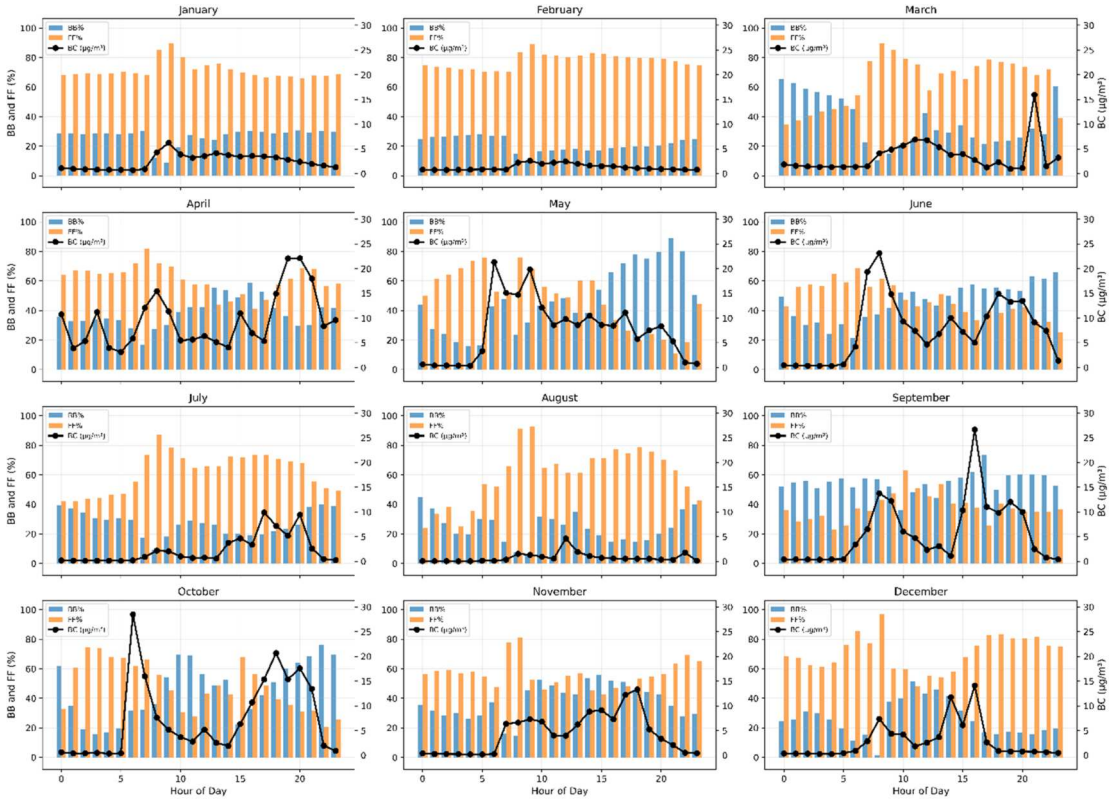

Figure 2. Monthly mean diurnal variation of BC concentration (μg m^{-3}) and the corresponding contributions from biomass burning (BB%) and fossil fuel (FF%). Each panel represents each month (January -December), showing hourly averages of BB% and FF% (stacked bars, left *y*-axis) along with BC concentration (black line, right *y*-axis).

other high-altitude Himalayan stations, such as 2.4 ± 2 μg m^{-3} in Gulmarg and 2.59 μg m^{-3} in Srinagar (Romshoo *et al* 2023), 2.706 μg m^{-3} in Kullu (Nair *et al* 2013), 1.93 ± 1.52 μg m^{-3} in Ranichauri (Pandey *et al* 2020), 9.759 ± 7.418 μg m^{-3} in Kathmandu, 4.765 ± 1.878 μg m^{-3} in Dhulikhel (Singh *et al* 2023) and 3.4 ± 1.9 μg m^{-3} in Darjeeling (Sarkar *et al* 2015). The mean diurnal variation shows a bimodal pattern (figure 2) with peaks in the morning (~08:00 IST, 9.14 μg m^{-3}) and evening (~18:00 IST, 8.67 μg m^{-3}). The lowest concentrations (~0.8 μg m^{-3}) occur during 00:00–05:00 IST, when anthropogenic activity is minimal and atmospheric conditions are more stable. The period of high BC concentrations aligns with the time during which the vehicular activity is high and the emissions from local tourism activities are higher. Yumthang experiences substantial tourist inflow, with peak traffic occurring in the morning and evening hours. This is also reflected in the FF% contribution during these hours. Additionally, local shops that rely heavily on wood burning for heating and cooking are the most active during this period, further contributing to elevated BC concentrations. This is visible in the BB% pattern in the months like July and August, when very few tourists visit and these shops remain mostly inactive, causing the BB and FF% ratio to fall significantly. Seasonal differences during pre-monsoon (Mar-May), monsoon (Jun-Aug), post-monsoon (Sep-Nov) and winter (Dec-Feb) season further support this interpretation. During the monsoon and winter months, tourism is minimal, leading to lower biomass burning activity. This is reflected by consistently higher FF% and comparatively lower BB% during these periods, as only essential vehicular movement such as limited local traffic persists. In contrast, in other months with higher tourist presence, greater variability in both BB% and FF% is evident due to increased cooking related biomass burning along with extensive vehicle movement. The diurnal pattern of BC concentration is also influenced by local meteorological factors, particularly boundary layer evolution and mountain-valley wind circulations (Krishna Moorthy *et al* 2003, Nair *et al* 2007). As the day advances and the land warms, an increase in BLH is observed around the study area which enhances vertical mixing, allowing pollutants to disperse more effectively (figure 3). The increase in BLH during the daytime lifts pollutants from lower down the valley, breaking the capping inversion formed overnight and resulting in the transfer of pollutants to higher altitudes. Upslope winds during the day, driven by the radiative heating, transport BC laden air parcels from lower in the valley to higher elevations. Similar diurnal variations have been reported at other high-altitude locations, including Qomolangma (Mt. Everest), Darjeeling, and sites in the Himalaya-Karakorum-Hindukush (HKH) region (Sarkar *et al* 2015, Chen *et al* 2018, Zeb *et al* 2020), where they have been attributed to enhanced local emissions and vertical mixing.

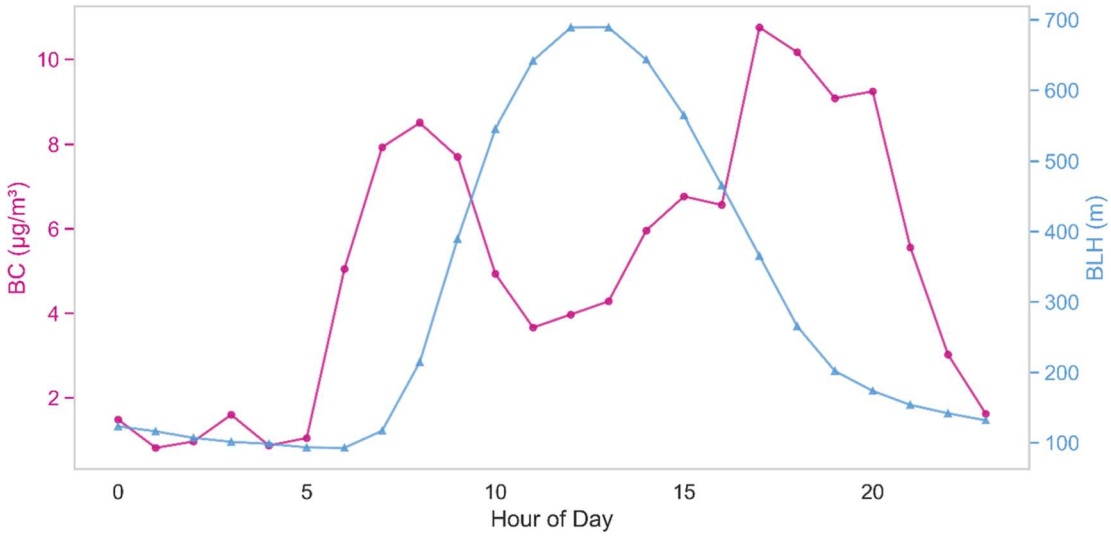

Figure 3. Diurnal variability of BC (pink line) and boundary layer height (BLH, blue line).

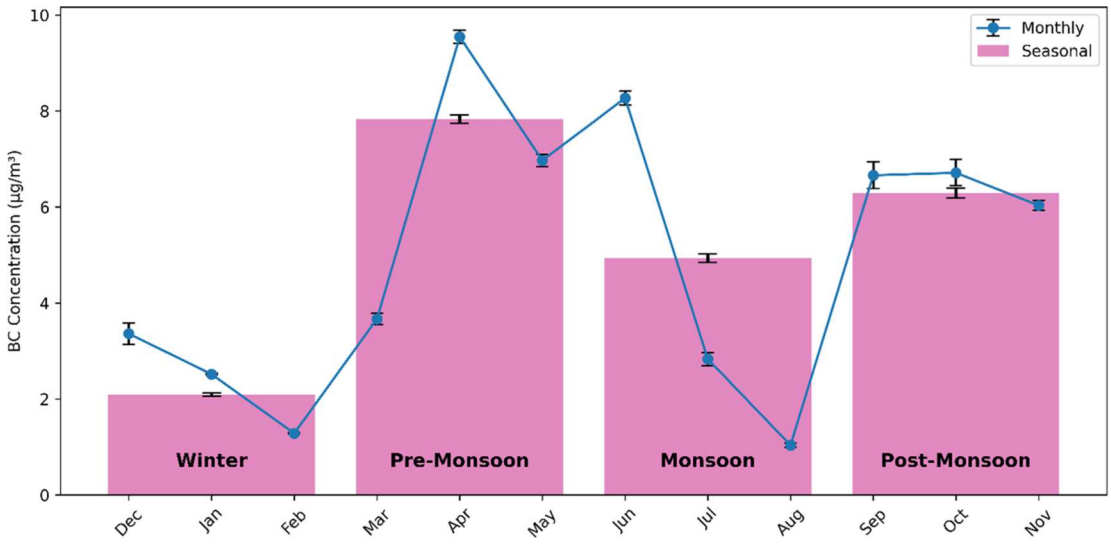

Figure 4. Monthly and seasonal variation of BC concentrations (µg m^{-3}) in the study area.

Table 1. List of datasets and instruments/models used in this study.

Data	Instruments/model
BC	Aethalometer
BLH	ERA5
RH	AWS
AOD, SSA, and AP	OPAC
Albedo	MODIS BRDF
water vapour	ERA5
Ozone	OMI

The monthly and seasonal mean concentration of BC is reported in figure 4 while their monthly statistics are given in table 2. BC concentration shows considerable variations at the study location, with the highest mean concentration during the month of April (9.55 µg m^{-3}) and the lowest in August (1.04 µg m^{-3}). The higher concentrations of BC during the pre-monsoon season in Yumthang valley are attributed to a combination of local and regional factors. Increased anthropogenic activities such as wood combustion, biomass

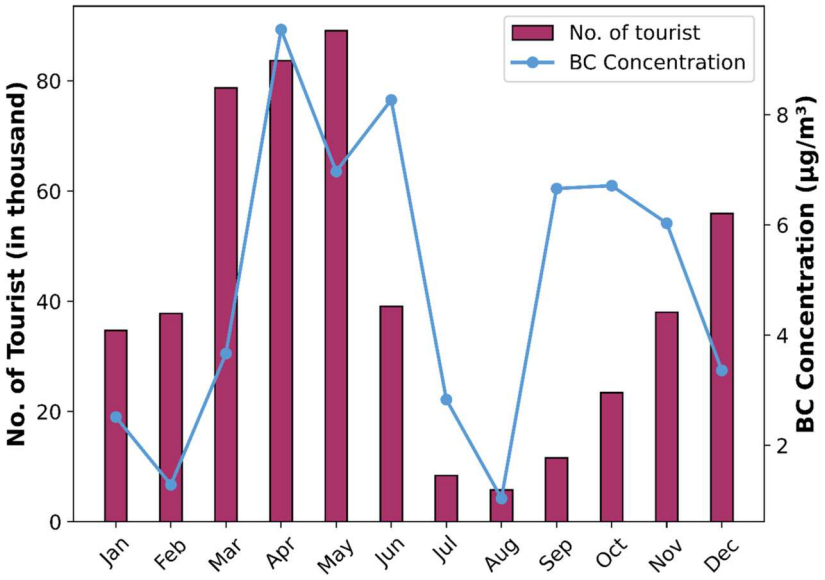

Figure 5. Relationship between tourist numbers (in thousands) and BC concentrations (μg m^{-3}) in Sikkim. (Source: Tourism Department, Govt. of Sikkim).

Table 2. Summary statistics of monthly mean BC concentration (μg m^{-3}) computed from 1-min BC measurements.

Month	Mean	Median	25%	75%	10%	90%
January	2.52	2.00	0.98	3.49	0.66	4.86
February	1.29	0.53	0.00	1.99	0.00	3.35
March	3.67	1.84	1.49	4.45	0.95	7.65
April	9.55	4.05	1.92	9.34	1.33	23.96
May	6.97	2.04	0.59	7.60	0.28	17.13
June	8.27	1.63	0.39	8.24	0.08	20.72
July	2.83	0.33	0.15	0.61	0.04	1.33
August	1.04	0.32	0.13	0.75	0.03	1.80
September	6.66	0.92	0.17	2.07	0.00	10.83
October	6.71	0.53	0.00	3.84	0.00	15.07
November	6.03	2.23	0.41	5.82	0.07	12.32
December	3.36	0.78	0.39	1.26	0.16	2.20

burning, and intensified traffic emissions from diesel-powered vehicles, driven by the influx of tourists (figure 5) amplify the BC concentration. The biomass burning contribution increases from about 20% in winter to roughly 40% in pre-monsoon as shown in figure 6, and this rise in BB% is accompanied by higher AAE values, together pointing to a stronger influence of biomass-derived carbonaceous aerosols at the site. Together with BB% a simultaneous increase of FF% is also observed during the period. Long-range transport also plays an important role; westerly winds carry aerosols, including emissions from agricultural burning in the IGP, as confirmed by CWT analysis (figure 7). These pollutants are advected to higher altitudes due to enhanced BLH and pre-monsoonal thermal convection (Lau *et al* 2006, Kumar *et al* 2011, Srivastava *et al* 2012, Vadrevu *et al* 2012), further elevating BC concentrations in the Himalayan region. Conversely, the sharp decrease in BC concentration in July and August as seen may be attributed to wet deposition from monsoonal precipitation. Monthly mean BC concentration reduced by more than half during these months compared to June which can be related to the onset of monsoon in Sikkim (IMD 2024). The monsoon season experiences a decline in BC concentrations due to below-cloud scavenging by heavy rainfall, which effectively washes out aerosols along the transport pathways. Although monsoon winds originate from the Arabian Sea and the Bay of Bengal, their extensive continental overpass results in significant aerosol removal before reaching high-altitude sites like Yumthang.

Additionally, minimal tourist activity during this period further reduces local emissions. The withdrawal of monsoon and increased tourist activity in September contribute to a sudden rise in BC concentration in the post-monsoon season. This increase is further influenced by valley wind transport mechanisms that modulate

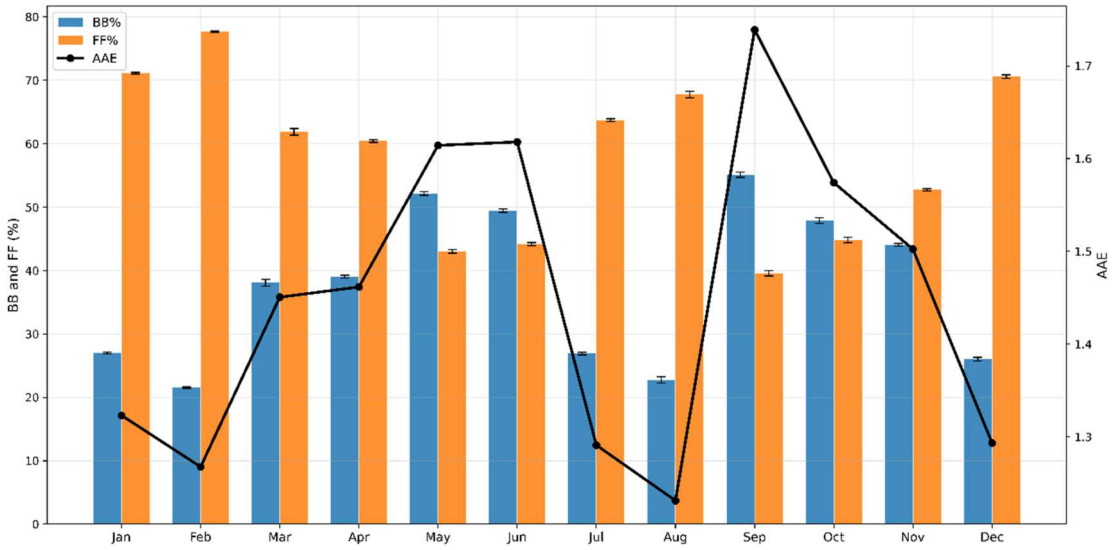

Figure 6. Monthly variation in the Biomass Burning (BB) and Fossil Fuel (FF) source contribution along with calculated AAE_{BC} values.

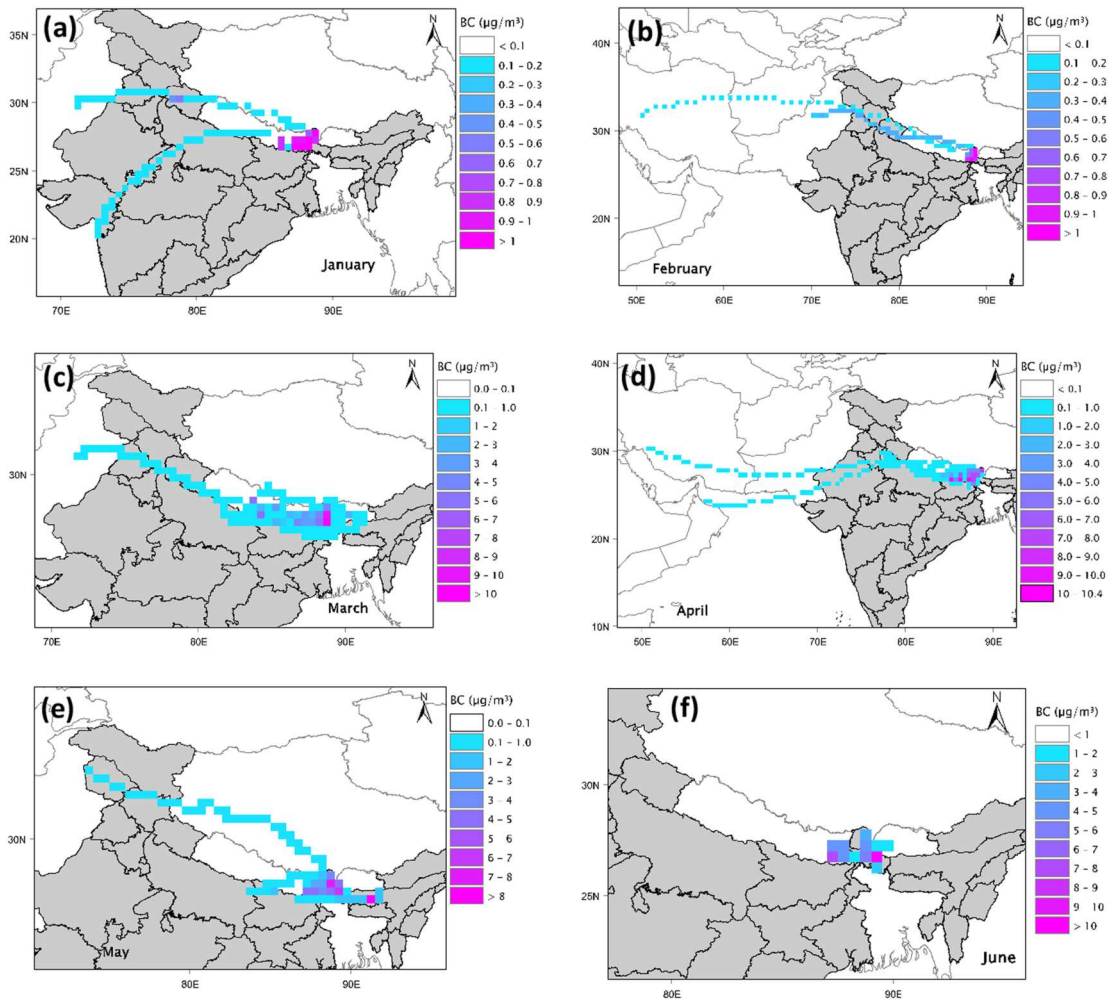

Figure 7. Concentration-Weighted Trajectory (CWT) plots showing the monthly transport paths and source regions affecting BC concentrations in Sikkim. Panels (a-l) correspond to January to December, respectively.

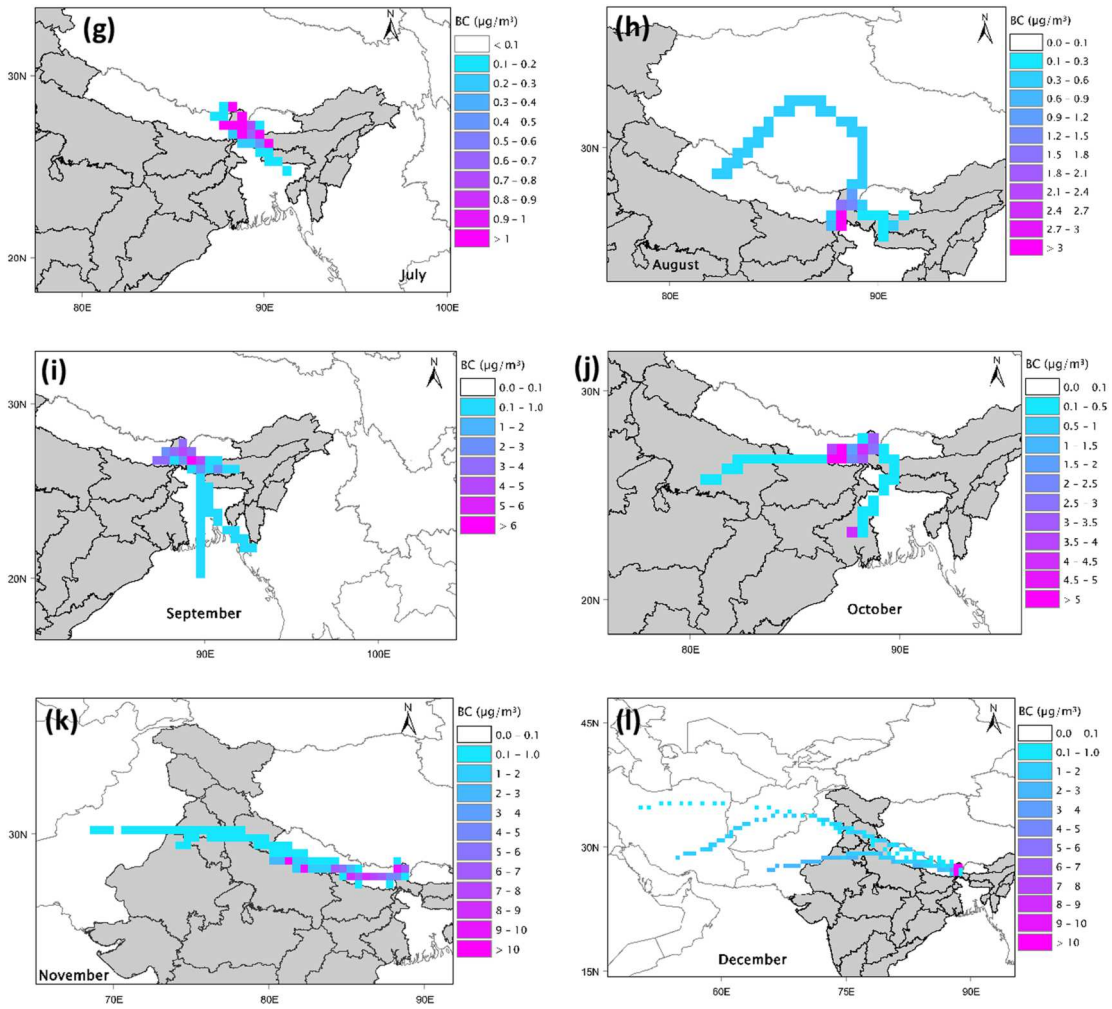

Figure 7. (Continued.)

pollutant influx at high-altitude stations (Dhungel *et al* 2018). In the post-monsoon season, BC concentration continues to rise moderately due to a combination of local emissions and long-range transportation of aerosols from crop-residue burning around the IGP and its adjoining region (Singh *et al* 2020). Though BC concentration in post-monsoon remains high, they are lower than those observed during pre-monsoon period. During the winter season, the decline in BC concentrations may arise from a reduced tourist influx as well as limited activities in the seasonal eateries. The confined nature of the local boundary layer, often at lower elevation further isolates the observational site from low-altitude pollution. Visual observations during winter mornings reveal smoke plumes from valley households remaining vertically constrained and dispersing horizontally, highlighting the limited vertical dispersion. However, with the onset of pre-monsoon, increased solar heating of the mountain surface intensifies thermal convection, facilitating the upward transport of BC into the troposphere (Nair *et al* 2007). Along with this, the local sources such as biomass burning and vehicle emissions are prominent, while the regional transport from the IGP is limited (Hyvärinen *et al* 2009, Dumka and Kaskaoutis 2014).

Similar monthly variability in BC concentrations has been observed at other Himalayan sites, including Qomolangma (Mt. Everest) (Chen *et al* 2018), Gangtok (Kumar *et al* 2024), Manora Peak (Dumka *et al* 2010) and Hanle (Babu *et al* 2011a). Although BC concentrations at Yumthang are significantly lower than in urban South Asian regions (Gogoi *et al* 2017, Vaishya *et al* 2017), its presence over highly reflective surfaces, such as snow-covered terrain, enhances their radiative forcing efficiency (Haywood and Shine 1995). The high standard deviation in BC concentrations, exceeding the mean value indicates the high variability during the study period. This can be attributed to localized short-term events that lead to sharp spikes in local concentrations. As the region is a popular tourist destination, periodic surges in visitor numbers increase the vehicular movement and associated fossil-fuel emissions, resulting in elevated BC. This pattern is evident throughout the months with high tourist load. The corresponding BB% and FF% further support this interpretation as shown in figure 6. During May, when tourist activity peaks, the difference between BB and FF narrows because biomass

burning also increases, largely due to wood burning for local energy requirements. In months with fewer tourists, the disparity between BB% and FF% becomes larger, reflecting reduced local activity. For most months, FF% dominates over BB% due to continuous vehicle movement. However, the seasonal pattern was more evident in BB%. The same may be revealed by the monthly averaged AAE values over the region. It is imperative to mention that higher BB% values correspond to low BC emissions and lower AAE values were mostly observed for high FF emissions (Hernández *et al* 2025). This may be the reason we have relatively lower value for AAE during the pre-monsoon season and high values in post monsoon when biomass burning was more.

4.2. Source apportionment and transport pathways

Contribution from biomass burning (BB) and fossil fuel (FF) to the total BC concentrations reveals significant seasonal and monthly variations, driven by both local and regional sources. BB contributes 37.74% to the overall BC annual mass on average, with a maximum contribution in September (55%) while FF contributes 57% annually, with maximum contribution in February (77%).

FF fractions generally remain between about 45%-80%, while BB varies from ∼20%-55%, indicating that fossil-fuel combustion provides a persistent background onto which biomass-burning emissions are superimposed. During pre-monsoon and early monsoon , BB% rises from winter values around 20%-30% to above 50% in May-June, with a corresponding drop in FF% to about 40%–45%. This BB enhancement coincides with elevated BC loadings at Yumthang which is also evident from the agricultural-residue burning over the IGP and Himalayan foothills, strengthening BB influence at central and western Himalayan regions (Sandeep *et al* 2022, Singh *et al* 2023). However, during the monsoon and winter season, BB contribution declines considerably due to reduced anthropogenic activity and limited aerosol dispersion under shallow boundary layer conditions. BC concentration during both seasons is largely associated with FF contribution from limited vehicular movement. FF is the major contributor, accounting for more than 60% of BC emissions, as seen in other Himalayan locations such as Nainital and Dehradun (Dumka *et al* 2014, Kant *et al* 2020).

Concentration Weighted Trajectory (CWT) analysis for source apportionment shows clear seasonal patterns in regional transport influencing BC concentrations in the Yumthang Valley. During the pre-monsoon and post-monsoon season , air masses from the IGP and Central Asia contribute to the high BC concentrations, but their contributions are relatively low in comparison to local sources. Similarly, local sources such as vehicular traffic and biomass burning for cooking and heating also become the dominant contributors in other seasons. It, therefore, highlights dual transport regimes: (i) spring and autumn transport from the IGP and Central Asia, enhancing pre-monsoon and post-monsoon BC, and (ii) local dominance throughout the year. Densely populated regions associated with large-scale biomass burning, vehicular emissions and industrial activities such as IGP, Middle Eastern nations, and Nepal emerge as source regions during long-range transportation (Gautam *et al* 2009, Vadrevu *et al* 2012). The widespread use of biofuels and frequent open biomass burning in IGP adds to the carbonaceous aerosol burden, making it a key source region affecting the Eastern Himalayan region (Sarkar *et al* 2017, 2019). While these studies highlight a strong contribution from the IGP, our results for the Sikkim Himalaya point to a predominantly local influence on BC levels. Although long-range transport from the IGP is known to affect the Eastern Himalayan region, as also reported by Sarkar *et al* (2017, 2019) and Arun *et al* (2021), our analysis indicates that localized emissions play a more dominant role than transported pollution at the Yumthang site. Regional modelling shows that South Asian emissions contribute a large share of the BC that reaches Himalayan glaciers, but it also indicates that local valley-scale sources become more important closer to the mountain front and in complex terrain (Li *et al* 2016). At Yumthang, the CWT maps highlight the strongest BC influence over Sikkim and nearby valleys, with only moderate contributions from the distant IGP and Central Asia. The observed diurnal peaks and the BB/FF source fractions also match local patterns in tourism, traffic, and household biomass burning. Taken together, this evidence indicates that the high and variable BC levels in Yumthang are mainly driven by local emissions, while long-range transport adds to the concentrations only during certain seasons.

4.3. BC direct radiative impact

BC concentrations play a significant role in augmenting the atmospheric radiative forcing (ARF), influencing regional climate dynamics. Monthly aerosol optical properties, including AOD, SSA, and AP, were simulated using the OPAC model at 550 nm for the study site. A good correlation (> 0.8) was observed between OPAC-derived AOD and CAMS reanalysis AOD for coincident months. Previous studies have also reported comparable agreement (Song *et al* 2021, Tiwary *et al* 2024). The OPAC-derived mean AOD over the study period was 0.10 ± 0.04 ranging from 0.02 to 0.29. These AOD values are lower than those reported from Mt. Abu during April 2007 (Das and Jayaraman 2011) and for HKH region (Zeb *et al* 2020) but are comparable to those reported at other high-altitude sites, such as 0.05 at QOMS (Xu *et al* 2016) and 0.04 at EVK2-CNR (Gobbi *et al* 2010). The lowest mean AOD values were observed in August (0.016) and February (0.021) whereas higher

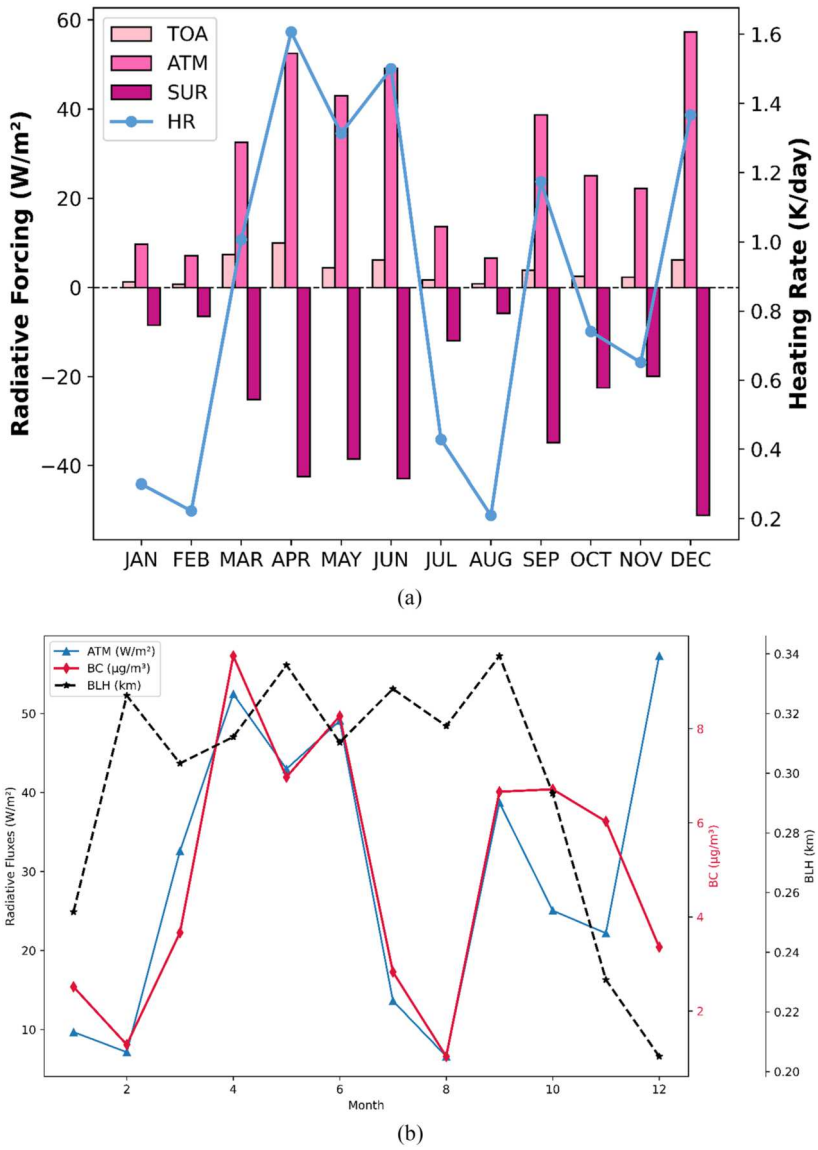

Figure 8. (a): Monthly variation of radiative forcing (W m^{-2}) at the surface (SUR), the top of the atmosphere (TOA), and within the atmosphere (ATM), along with the atmospheric heating rate (K/day) over the study area. (b): Monthly variation of atmospheric radiative forcing, black carbon, and boundary layer height over the observation site. The blue line shows atmospheric radiative forcing (ATM, W m^{-2}) on the left axis, the red line indicates near-surface black carbon concentration (BC, µg m^{-3}) on the right axis, and the black dashed line represents boundary layer height (BLH, km) on the secondary right axis, illustrating their co-variability across the year.

values observed in April (0.139) and June (0.131), in agreement with the corresponding seasonal variation in BC concentrations as discussed above. The monthly mean BC-induced ARF at surface (SUR) within the atmosphere (ATM), and the top-of-atmosphere (TOA) with corresponding heating rates (HR) are shown in figure 8(a). ARF at TOA was found to be maximum during April (9.98 W m^{-2}) and minimum (0.70 W m^{-2}) during February at Yumthang. SUR forcing showed a reduction in incoming solar radiation, ranging from −5.79 W m^{-2} in August and −51.09 W m^{-2} in December. The presence of atmospheric BC decreases the amount of solar radiation reaching the Earth's surface, resulting in negative SUR forcing and surface cooling, while its strong absorptive properties contribute to positive TOA forcing by trapping solar radiation in the atmosphere. The BC-induced ARF shows strong monthly variability within the ATM with a maximum in December (57.27 W m^{-2}) and minimum during August (6.60 W m^{-2}). The Atmospheric forcing (ATM) was positive, peaking in Dec (57.27 W m^{-2}), though this is an unusually high value likely reflecting local inversion conditions and enhanced winter absorption (Srivastava and Ramachandran 2013). For comparison, typical Himalayan sites report 15-30 W m^{-2} (Babu *et al* 2011, Dumka *et al* 2010), suggesting Yumthang experiences episodic forcing intensification.

The positive ATM forcing is largely due to the absorption of solar radiation by the BC concentration in the atmosphere over the region. Similar observations have also been reported in the IGP region (Srivastava and

Ramachandran 2013). The variability in ARF is modulated by additional factors such as the concentration and composition of coexisting aerosols, AOD, wind speed, site elevation, surface characteristics, and prevailing meteorological conditions. Higher ARF values within the ATM were observed during pre-monsoon, moderate during the monsoon and winter and lower in the post-monsoon period. It is evident from figure 8(b) that during December month BLH layer is extremely low resulting in high ATM forcing due to relatively enhanced BC concentration in the lower boundary layer. Therefore, a substantial atmospheric and surface radiative forcing was observed during November and December. The pronounced differences between TOA and SUR forcing, particularly in winter, suggest that a significant portion of solar radiation is absorbed and retained within the atmosphere, contributing to enhanced atmospheric heating. This strong absorption of solar radiation plays a crucial role in the alteration of the thermodynamic conditions in the atmosphere affecting the atmospheric circulation (Lau and Kim 2006). BC induced heating rates were found to range between 0.21 K/day to 1.61 K/day. The heating rates show moderate correlation with the BC concentrations. Positive heating rates in high-altitude regions affect the cryospheric system leading to increased rates of glacier and snow melts. BC plays an important role in the regional energy balance and hence long-term monitoring is a necessary input for improving climate models and better understanding the region's climate.

5. Conclusion

This study presents two years (May 2022–April 2024) of continuous black carbon (BC) observations from Yumthang Valley in Eastern Himalaya one of the few high-altitude datasets available for this region. The results reveal substantial seasonal and diurnal variability, with concentrations ranging from 1.04 $\mu g\ m^{-3}$ (August) to 9.55 $\mu g\ m^{-3}$ (April). Distinct bimodal diurnal peaks in the morning and evening correspond to tourist inflows, local wood combustion, and boundary layer evolution. Seasonal maxima in the pre-monsoon reflect long-range transport of biomass burning plumes from the IGP, while minima during the monsoon highlight efficient wet scavenging. Source apportionment indicates that fossil fuels (57%) are the dominant contributor, particularly in winter, while biomass burning (38%) is most influential during post-harvest periods. CWT analysis confirms Yumthang's dual exposure to local anthropogenic sources and regional inflow from IGP and Central Asia . BC-induced radiative forcing showed strong seasonal contrasts. TOA forcing peaked at ∼10 $W\ m^{-2}$ in April, while surface forcing was strongly negative in winter (−51 $W\ m^{-2}$). The resulting atmospheric forcing (ATM) reached up to 57 $W\ m^{-2}$ in December, significantly higher than typical Himalayan averages, reflecting episodic wintertime trapping and enhanced absorption. The mean atmospheric heating rate was ∼0.83 K/day, with maxima of 1.6 K/day, values consistent with those reported across the Himalaya–Karakoram–Hindukush region. Importantly, in snow-covered conditions, the snow-albedo feedback likely enhances effective forcing, accelerating melt. These findings demonstrate that Yumthang Valley is highly vulnerable to both transported and locally generated BC, with implications for cryosphere health, hydrological regimes, and regional climate stability. The increasing role of tourism underscores the need for targeted mitigation policies, such as improved vehicle emission standards and sustainable tourism practices, . Long-term BC and co-emitted aerosol monitoring in Eastern Himalaya is essential to improve climate projections, inform regional adaptation strategies, and safeguard critical glacier-fed water resources.

Acknowledgments

The authors acknowledge the ANRF, Govt. of India, for the project on Mass Size distribution and chemical characteristics of ambient aerosols over Sikkim Himalayas and its impact on the Cryosphere (CRG/2023/008852 dated:15/05/2024) and the DST's Centre of Excellence established by Department of Science and Technology, Government of India (DST/CCP/CoE/186/2019(G), dated 03/03/2020) for the instrumentation and facilities for the work. We also acknowledge the anonymous persons who so ever have helped and supported for the Black Carbon data collection. The authors also acknowledge NOAA and TrajStat (www.meteothink.org/products/trajstat.html) for their open-access software packages.

Conflict of interest

No conflict of interest.

Data availability statement

The data cannot be made publicly available upon publication because they are owned by a third party and the terms of use prevent public distribution. The data that support the findings of this study are available upon reasonable request from the authors.

Author contributions

Aparna Gupta 0000-0002-8517-9913
Conceptualization (lead), Data curation (equal), Formal analysis (lead), Methodology (lead), Software (lead), Validation (equal), Visualization (lead), Writing – original draft (lead), Writing – review & editing (lead)

Rakesh Kumar Ranjan 0000-0001-8745-3923
Conceptualization (equal), Funding acquisition (equal), Methodology (equal), Project administration (equal), Resources (equal), Supervision (equal), Validation (equal), Writing – review & editing (equal)

Vrinda Anand
Formal analysis (equal), Methodology (supporting), Software (equal), Validation (equal), Writing – review & editing (equal)

Abhilash Panicker
Formal analysis (equal), Investigation (equal), Methodology (supporting), Supervision (equal), Writing – review & editing (supporting)

Rajeev Rajak 0000-0001-7672-6631
Data curation (equal), Formal analysis (supporting), Methodology (supporting), Writing – review & editing (supporting)

Khushboo Sharma
Data curation (supporting), Methodology (supporting), Writing – review & editing (supporting)

Bidyutjyoti Baruah
Data curation (supporting), Methodology (supporting), Writing – review & editing (supporting)

Ankita Roy
Data curation (supporting), Methodology (supporting), Writing – review & editing (supporting)

Shruti Dutta
Formal analysis (supporting), Supervision (equal), Writing – review & editing (equal)

Amit Prakash
Formal analysis (supporting), Supervision (equal), Writing – review & editing (equal)

References

Agrawal A, Sharma A R and Tayal S 2014 Assessment of regional climatic changes in the Eastern Himalayan region: a study using multi-satellite remote sensing data sets *Environ. Monit. Assess.* **186** 6521–36

Arun B S, Aswini A R, Gogoi M M, Hegde P, Kumar Kompalli S, Sharma P and Suresh Babu S 2019 Physico-chemical and optical properties of aerosols at a background site (~4 km a.s.l.) in the western Himalayas *Atmos. Environ.* **218** 117017

Arun B S, Gogoi M M, Borgohain A, Hegde P, Kundu S S and Babu S S 2021 Role of sulphate and carbonaceous aerosols on the radiative effects of aerosols over a remote high-altitude site Lachung in the Eastern Himalayas *Atmos. Res.* **263** 105799

Babu S S *et al* 2011a High altitude (~4520 m amsl) measurements of black carbon aerosols over western trans-Himalayas: Seasonal heterogeneity and source apportionment: HIGH ALTITUDE MEASUREMENT OF BC AEROSOLS *Journal of Geophysical Research: Atmospheres* **116**

Babu S S, Moorthy K K, Manchanda R K, Sinha P R, Satheesh S K, Vajja D P, Srinivasan S and Kumar V H A 2011b Free tropospheric black carbon aerosol measurements using high altitude balloon: Do BC layers build 'their own homes' up in the atmosphere?: Free tropospheric black carbon aerosol *Geophys. Res. Lett.* **38**

Babu S S, Satheesh S K, Moorthy K K, Dutt C B S, Nair V S, Alappattu D P and Kunhikrishnan P K 2008 Aircraft measurements of aerosol black carbon from a coastal location in the north-east part of peninsular India during ICARB *J. Earth Syst. Sci.* **117** 263–71

Bond T C, Bhardwaj E, Dong R, Jogani R, Jung S, Roden C, Streets D G and Trautmann N M 2007 Historical emissions of black and organic carbon aerosol from energy-related combustion, 1850–2000 *Global Biogeochem. Cycles* **21** 2006GB002840

Bond T C *et al* 2013 Bounding the role of black carbon in the climate system: A scientific assessment *Journal of Geophysical Research: Atmospheres* **118** 5380–552
Campagnolo M L, Sun Q, Liu Y, Schaaf C, Wang Z and Román M O 2016 Estimating the effective spatial resolution of the operational BRDF, albedo, and nadir reflectance products from MODIS and VIIRS *Remote Sens. Environ.* **175** 52–64
Chaubey J P, Krishna Moorthy K, Suresh Babu S and Nair V S 2011 The optical and physical properties of atmospheric aerosols over the Indian Antarctic stations during southern hemispheric summer of the International Polar Year 2007–2008 *Ann. Geophys.* **29** 109–21
Chen X, Kang S, Cong Z, Yang J and Ma Y 2018 Concentration, temporal variation, and sources of black carbon in the Mt. Everest region retrieved by real-time observation and simulation *Atmos. Chem. Phys.* **18** 12859–75
Das S K and Jayaraman A 2011 Role of black carbon in aerosol properties and radiative forcing over western India during premonsoon period *Atmos. Res.* **102** 320–34
Déry S J and Brown R D 2007 Recent Northern Hemisphere snow cover extent trends and implications for the snow-albedo feedback *Geophys. Res. Lett.* **34** 2007GL031474
Dhungel S, Kathayat B, Mahata K and Panday A 2018 Transport of regional pollutants through a remote trans-Himalayan valley in Nepal *Atmos. Chem. Phys.* **18** 1203–16
Diaz Resquin M, Santágata D, Gallardo L, Gómez D, Rössler C and Dawidowski L 2018 Local and remote black carbon sources in the Metropolitan Area of Buenos Aires *Atmos. Environ.* **182** 105–14
Drinovec L *et al* 2015 The "dual-spot" Aethalometer: an improved measurement of aerosol black carbon with real-time loading compensation *Atmos. Meas. Tech.* **8** 1965–79
Dumka U C, Moorthy K K, Kumar R, Hegde P, Sagar R, Pant P, Singh N and Babu S S 2010 Characteristics of aerosol black carbon mass concentration over a high altitude location in the Central Himalayas from multi-year measurements *Atmos. Res.* **96** 510–21
Dumka U C and Kaskaoutis D G 2014 In-situ measurements of aerosol properties and estimates of radiative forcing efficiency over Gangetic-Himalayan region during the GVAX field campaign *Atmos. Environ.* **94** 96–105
Dumka U C, Kaskaoutis D G, Srivastava M K and Devara P C S 2014 Scattering and absorption properties of near-surface aerosol over Gangetic–Himalayan region: the role of boundary layer dynamics and long-range transport *Aerosols/Field Measurements/ Troposphere/Physics (Physical Properties and Processes)* **15** 1555–72
Flanner M G, Zender C S, Hess P G, Mahowald N M, Painter T H, Ramanathan V and Rasch P J 2009 Springtime warming and reduced snow cover from carbonaceous particles *Atmos. Chem. Phys.* **9** 2481–97
Gautam R, Hsu N C, Lau K -M, Tsay S -C and Kafatos M 2009 Enhanced pre-monsoon warming over the Himalayan-Gangetic region from 1979 to 2007 *Geophys. Res. Lett.* **36** GL037641
Gobbi G P, Angelini F, Bonasoni P, Verza G P, Marinoni A and Barnaba F 2010 Sunphotometry of the 2006–2007 aerosol optical/radiative properties at the Himalayan Nepal Climate Observatory-Pyramid (5079 m a.s.l.) *Atmos. Chem. Phys.* **10** 11209–21
Gogoi M M *et al* 2017 Radiative effects of absorbing aerosols over northeastern India: Observations and model simulations *Journal of Geophysical Research: Atmospheres* **122** 1132–57
Gul C, Mahapatra P S, Kang S, Singh P K, Wu X, He C, Kumar R, Rai M, Xu Y and Puppala S P 2021 Black carbon concentration in the central Himalayas: Impact on glacier melt and potential source contribution *Environ. Pollut.* **275** 116544
Haywood J M and Shine K P 1995 The effect of anthropogenic sulfate and soot aerosol on the clear sky planetary radiation budget *Geophys. Res. Lett.* **22** 603–6
Helin A *et al* 2021 Variation of absorption Ångström exponent in aerosols from different emission sources *Journal of Geophysical Research: Atmospheres* **126** e2020JD034094
Hernández I M, González L T, Mancilla Y, Longoria-Rodríguez F E, Alfaro J M, Pérez-Rodríguez M and Mendoza A 2025 Assessing black carbon sources with aethalometer data and ambient ΔBC/ΔCO ratios analysis *Sci. Rep.* **15** 35716
Hess M., Koepke P. and Schult I. 1998 Optical Properties of Aerosols and Clouds: The Software Package OPAC *Bull. Am. Meteorol. Soc.* **79** 831–44
Hsu Y-K, Holsen T M and Hopke P K 2003 Comparison of hybrid receptor models to locate PCB sources in Chicago *Atmos. Environ.* **37** 545–62
Hyvärinen A -P, Lihavainen H, Komppula M, Sharma V P, Kerminen V -M, Panwar T S and Viisanen Y 2009 Continuous measurements of optical properties of atmospheric aerosols in Mukteshwar, northern India *Journal of Geophysical Research: Atmospheres* **114** 2008JD011489
IMD 2024 *Review of Seasonal Forecast of Monsoon 2023* (https://imdpune.gov.in/imsp/presentations/18/AMW_2024_LRF_sreejith_18_March_2024.pdf)
IPCC 2013 *Climate Change 2013—The Physical Science Basis: Working Group I Contribution to the Fifth Assessment Report of the Intergovernmental Panel on Climate Change* 1st edn, ed T F Stocker *et al* (Cambridge University Press) (https://doi.org/10.1017/CBO9781107415324)
Kääb A, Berthier E, Nuth C, Gardelle J and Arnaud Y 2012 Contrasting patterns of early twenty-first-century glacier mass change in the Himalayas *Nature* **488** 495–8
Kakkar A, Rai P K, Mishra V N and Singh P 2022 Decadal trend analysis of rainfall patterns of past 115 years and its impact on Sikkim, India *Remote Sensing Applications: Society and Environment* **26** 100738
Kang S *et al* 2022 Black carbon and organic carbon dataset over the Third Pole *Earth System Science Data* **14** 683–707
Kant Y, Shaik D S, Mitra D, Chandola H C, Babu S S and Chauhan P 2020 Black carbon aerosol quantification over north-west Himalayas: Seasonal heterogeneity, source apportionment and radiative forcing *Environ. Pollut.* **257** 113446
Kirchstetter T W, Novakov T and Hobbs P V 2004 Evidence that the spectral dependence of light absorption by aerosols is affected by organic carbon *Journal of Geophysical Research: Atmospheres* **109** 2004JD004999
Koch D and Del Genio A D 2010 Black carbon semi-direct effects on cloud cover: review and synthesis *Atmos. Chem. Phys.* **10** 7685–96
Krishna Moorthy K, Pillai P S and Suresh Babu S 2003 Influence of changes in the prevailing synoptic conditions on the response of aerosol characteristics to land- and sea-breeze circulations at a coastal station *Boundary Layer Meteorol.* **108** 145–61
Krishna R K, Panicker A S, Yusuf A M and Ullah B G 2019 On the Contribution of Particulate Matter (PM2.5) to Direct Radiative Forcing over Two Urban Environments in India *Aerosol Air Qual. Res.* **19** 399–410
Kumar P *et al* 2024 Measurement report: Intra-annual variability of black carbon and brown carbon and their interrelation with meteorological conditions over Gangtok, Sikkim *Atmos. Chem. Phys.* **24** 11585–601
Kumar R, Naja M, Satheesh S K, Ojha N, Joshi H, Sarangi T, Pant P, Dumka U C, Hegde P and Venkataramani S 2011 Influences of the springtime northern Indian biomass burning over the central Himalayas *J. Geophys. Res.* **116** D19302
Lamarque J-F *et al* 2010 Historical (1850–2000) gridded anthropogenic and biomass burning emissions of reactive gases and aerosols: methodology and application *Atmos. Chem. Phys.* **10** 7017–39

Lapere R, Huneeus N, Mailler S, Menut L and Couvidat F 2023 Meteorological export and deposition fluxes of black carbon on glaciers of the central Chilean Andes *Atmos. Chem. Phys.* **23** 1749–68
Lau K -M and Kim K -M 2006 Observational relationships between aerosol and Asian monsoon rainfall, and circulation *Geophys. Res. Lett.* **33** GL027546
Lau K M, Kim M K and Kim K M 2006 Asian summer monsoon anomalies induced by aerosol direct forcing: the role of the Tibetan Plateau *Clim. Dyn.* **26** 855–64
Lawrence M G and Lelieveld J 2010 Atmospheric pollutant outflow from southern Asia: a review *Atmos. Chem. Phys.* **10** 11017–96
Li C, Bosch C, Kang S, Andersson A, Chen P, Zhang Q, Cong Z, Chen B, Qin D and Gustafsson Ö 2016 Sources of black carbon to the Himalayan–Tibetan Plateau glaciers *Nat. Commun.* **7** 12574
Liou K 2002 *An Introduction to Atmospheric Radiation* (*International Geophysics Series*) vol 84 (Academic) p 392 https://cir.nii.ac.jp/crid/1570572699506021504
Magee Scientific 2018 *Aethalometer® Model AE33 User Manual* (Magee Scientific)
Marinoni A *et al* 2010 Aerosol mass and black carbon concentrations, a two year record at NCO-P (5079 m, Southern Himalayas) *Atmos. Chem. Phys.* **10** 8551–62
Ménégoz M *et al* 2014 Snow cover sensitivity to black carbon deposition in the Himalayas: From atmospheric and ice core measurements to regional climate simulations *Atmos. Chem. Phys.* **14** 4237–49
Ménégoz M, Krinner G, Balkanski Y, Cozic A, Boucher O and Ciais P 2013 Boreal and temperate snow cover variations induced by black carbon emissions in the middle of the 21st century *The Cryosphere* **7** 537–54
Menon S, Koch D, Beig G, Sahu S, Fasullo J and Orlikowski D 2010 Black carbon aerosols and the third polar ice cap *Atmos. Chem. Phys.* **10** 4559–71
Nair V S, Babu S S, Moorthy K K, Sharma A K, Marinoni A and None A 2013 Black carbon aerosols over the Himalayas: direct and surface albedo forcing *Tellus B: Chemical and Physical Meteorology* **65** 19738
Nair V S *et al* 2007 Wintertime aerosol characteristics over the Indo-Gangetic Plain (IGP): Impacts of local boundary layer processes and long-range transport *Journal of Geophysical Research: Atmospheres* **112** 2006JD008099
Ohara T, Akimoto H, Kurokawa J, Horii N, Yamaji K, Yan X and Hayasaka T 2007 An Asian emission inventory of anthropogenic emission sources for the period 1980–2020 *Atmos. Chem. Phys.* **7** 4419–44
Pandey C P, Singh J, Soni V K and Singh N 2020 Yearlong first measurements of black carbon in the western Indian Himalaya: influences of meteorology and fire emissions *Atmospheric Pollution Research* **11** 1199–210
Rahimi S, Liu X, Zhao C, Lu Z and Lebo Z J 2020 Examining the atmospheric radiative and snow-darkening effects of black carbon and dust across the Rocky Mountains of the United States using WRF-Chem *Atmos. Chem. Phys.* **20** 10911–35
Ramachandran S and Rajesh T A 2007 Black carbon aerosol mass concentrations over Ahmedabad, an urban location in western India: comparison with urban sites in Asia, Europe, Canada, and the United States *Journal of Geophysical Research: Atmospheres* **112** 2006JD007488
Ramanathan V and Carmichael G 2008 Global and regional climate changes due to black carbon *Nat. Geosci.* **1** 221–7
Ricchiazzi P, Gautier C, Yang S and Sowle D 1998 SBDART: a research and teaching software tool for plane-parallel radiative transfer in the earth's atmosphere *Bull. Am. Meteorol. Soc.* **79** 2101–14
Romshoo B, Bhat M A and Habib G 2023 Black carbon in contrasting environments in India: Temporal variability, source apportionment and radiative forcing *Atmos. Environ.* **302** 119734
Romshoo S A, Murtaza K O, Shah W, Ramzan T, Ameen U and Bhat M H 2022 Anthropogenic climate change drives melting of glaciers in the Himalaya *Environmental Science and Pollution Research* **29** 52732–51
Rowe P M *et al* 2019 Black carbon and other light-absorbing impurities in snow in the Chilean Andes *Sci. Rep.* **9** 4008
Sandeep K, Panicker A S, Gautam A S, Beig G, Gandhi N, S S, Shankar R and Nainwal H C 2022 Black carbon over a high altitude Central Himalayan Glacier: Variability, transport, and radiative impacts *Environ. Res.* **204** 112017
Sarkar C, Chatterjee A, Majumdar D, Roy A, Srivastava A, Ghosh S K and Raha S 2017 How the atmosphere over Eastern Himalaya, India is polluted with carbonyl compounds? Temporal variability and identification of sources *Aerosol Air Qual. Res.* **17** 2206–23
Sarkar C, Chatterjee A, Singh A K, Ghosh S K and Raha S 2015 Characterization of black carbon aerosols over Darjeeling—a high altitude Himalayan Station in Eastern India *Aerosol Air Qual. Res.* **15** 465–78
Sarkar C, Roy A, Chatterjee A, Ghosh S K and Raha S 2019 Factors controlling the long-term (2009–2015) trend of PM2.5 and black carbon aerosols at eastern Himalaya, India *Sci. Total Environ.* **656** 280–96
Satheesh S K, Moorthy K K, Babu S S, Vinoj V and Dutt C B S 2008 Climate implications of large warming by elevated aerosol over India *Geophys. Res. Lett.* **35** 2008GL034944
Satheesh S K and Srinivasan J 2006 A method to estimate aerosol radiative forcing from spectral optical depths *J. Atmos. Sci.* **63** 1082–92
Sharma K, Ranjan R K, Lohar S, Sharma J, Rajak R, Gupta A, Prakash A and Pandey A K 2022 Black carbon concentration during spring season at high altitude Urban Center in Eastern Himalayan Region of India *Asian Journal of Atmospheric Environment* **16** 2021149
Singh G K, Choudhary V, Gupta T and Paul D 2020 Investigation of size distribution and mass characteristics of ambient aerosols and their combustion sources during post-monsoon in northern India *Atmospheric Pollution Research* **11** 170–8
Singh P K, Adhikary B, Chen X, Kang S, Poudel S P, Tashi T, Goswami A and Puppala S P 2023 Variability of ambient black carbon concentration in the Central Himalaya and its assessment over the Hindu Kush Himalayan region *Sci. Total Environ.* **858** 160137
Song S-K, Choi Y-N, Choi Y, Flynn J and Sadeghi B 2021 Characteristics of aerosol chemical components and their impacts on direct radiative forcing at urban and suburban locations in Southeast Texas *Atmos. Environ.* **246** 118151
Srivastava A K, Singh S, Pant P and Dumka U C 2012 Characteristics of black carbon over Delhi and Manora Peak—a comparative study *Atmos. Sci. Lett.* **13** 223–30
Srivastava R and Ramachandran S 2013 The mixing state of aerosols over the Indo-Gangetic Plain and its impact on radiative forcing *Q. J. R. Meteorolog. Soc.* **139** 137–51
Srivastava R, Ramachandran S, Rajesh T A and Kedia S 2011 Aerosol radiative forcing deduced from observations and models over an urban location and sensitivity to single scattering albedo *Atmos. Environ.* **45** 6163–71
Stohl A *et al* 2006 Pan-Arctic enhancements of light absorbing aerosol concentrations due to North American boreal forest fires during summer 2004 *Journal of Geophysical Research: Atmospheres* **111** 2006JD007216
Strahler A H, Muller J, Lucht W, Schaaf C, Tsang T, Gao F, Li X, Lewis P and Barnsley M J 1999 MODIS BRDF/albedo product: algorithm theoretical basis document version 5.0 *MODIS Documentation* **23** 42–7
Tinorua S, Denjean C, Nabat P, Bourrianne T, Pont V, Gheusi F and Leclerc E 2024 Higher absorption enhancement of black carbon in summer shown by 2-year measurements at the high-altitude mountain site of Pic du Midi Observatory in the French Pyrenees *Atmos. Chem. Phys.* **24** 1801–24

Tiwary P, Kukreti S, Shridhar V, Abhinav A, Rana S, Arunachalam K and Singh V 2024 Assessment of Black Carbon, optical properties and aerosol radiative forcing at Pranmati basin Himalayan critical zone observatory *Sci. Total Environ.* **933** 173050

Tomasi C *et al* 2007 Aerosols in polar regions: a historical overview based on optical depth and *in situ* observations *Journal of Geophysical Research: Atmospheres* **112** 2007JD008432

Vadrevu K P, Ellicott E, Giglio L, Badarinath K V S, Vermote E, Justice C and Lau W K M 2012 Vegetation fires in the himalayan region—Aerosol load, black carbon emissions and smoke plume heights *Atmos. Environ.* **47** 241–51

Vaishya A, Singh P, Rastogi S and Babu S S 2017 Aerosol black carbon quantification in the central Indo-Gangetic plain: seasonal heterogeneity and source apportionment *Atmos. Res.* **185** 13–21

Wang J, De Leeuw G, Niu S and Kang H 2019 Contrasting aerosol optical characteristics and source regions during summer and winter pollution episodes in Nanjing, China *Remote Sensing* **11** 1696

Wang Q *et al* 2016 Physicochemical characteristics of black carbon aerosol and its radiative impact in a polluted urban area of China *Journal of Geophysical Research: Atmospheres* **121**

Wang Y Q, Zhang X Y and Draxler R R 2009 TrajStat: GIS-based software that uses various trajectory statistical analysis methods to identify potential sources from long-term air pollution measurement data *Environ. Modelling Softw.* **24** 938–9

Weingartner E, Saathoff H, Schnaiter M, Streit N, Bitnar B and Baltensperger U 2003 Absorption of light by soot particles: determination of the absorption coefficient by means of aethalometers *J. Aerosol Sci.* **34** 1445–63

Xu B *et al* 2009 Black soot and the survival of Tibetan glaciers *Proc. Natl Acad. Sci.* **106** 22114–8

Xu Y, Ramanathan V and Washington W M 2016 Observed high-altitude warming and snow cover retreat over Tibet and the Himalayas enhanced by black carbon aerosols *Atmos. Chem. Phys.* **16** 1303–15

Zeb B, Alam K, Nasir J, Mansha M, Ahmad I, Bibi S, Malik S M and Ali M 2020 Black Carbon aerosol characteristics and radiative forcing over the high altitude glacier region of Himalaya-Karakorum-Hindukush *Atmos. Environ.* **238** 117711

Zhao Z *et al* 2017 Black carbon aerosol and its radiative impact at a high-altitude remote site on the southeastern Tibet Plateau *Journal of Geophysical Research: Atmospheres* **122** 5515–30

Zotter P, Herich H, Gysel M, El-Haddad I, Zhang Y, Močnik G, Hüglin C, Baltensperger U, Szidat S and Prévôt A S H 2017 Evaluation of the absorption Ångström exponents for traffic and wood burning in the Aethalometer-based source apportionment using radiocarbon measurements of ambient aerosol *Atmos. Chem. Phys.* **17** 4229–49